Materials Transactions, Vol. 44, No. 3 (2003) pp. 337 to 343

Effects of Impurities on an Al Grain Boundary

Guang-Hong Lu[1,2], Akira Suzuki[3], Akira Ito[4], Masanori Kohyama[5] and Ryoichi Yamamoto[1]

[1]*Institute of Industrial Science, University of Tokyo, Tokyo 106-8558, Japan*
[2]*School of Science, Beijing University of Aeronautics & Astronautics, Beijing 100083, P. R. China*
[3]*School of Computational Sciences, George Mason University, Virginia 22030-4444, USA*
[4]*Sony Corporation Core Technology & Network Company, Yokohama Research Center, Yokohama 240-0036, Japan*
[5]*Special Division of Green life Technology, National Institute of Advanced Industrial Science and Technology, Ikeda 563-8577, Japan*

The atomic and electronic structures of the Al $\Sigma = 9$ tilt grain boundary with segregated impurity atoms have been calculated by the first-principles pseudopotential method based on the local density functional theory. Effects of impurities of group I (Na), group II (Ca), group IV (Si) and group VI (S) have been examined. For the Na and Ca segregation cases, the impurity-Al interactions seem to have metallic characters. However, the boundary expands substantially and the charge density decreases significantly over the boundary. Thus these impurities should cause weaker intergranular adhesion. For both the Si and S segregation cases, the charge density increases around the impurity atom. The Si atom forms the covalent-metallic character mixing bonds with neighboring Al atoms. Such strong and directional bonds should prevent the rearrangement of atoms under stresses. However, the S atom forms such a strong bond with only one neighbor, differently from the Si case. It can be said that each impurity has various effects on the local atomic and electronic structure of an Al grain boundary according to the nature of each species, which seems to dominate the mechanism of embrittlement.

(Received November 18, 2002; Accepted December 26, 2002)

Keywords: *aluminium grain boundary, impurity segregation, embrittlement, first-principles calculation*

1. Introduction

Two models have been proposed in understanding the mechanism of impurity-promoted grain boundary embrittlement in polycrystalline metals. One is a 'decohesion model', in which, the metal-impurity or metal-metal cohesion is weakened by impurity segregation at grain boundaries. Related to this is an earlier speculation that hydrogen embrittlement results from a transfer of hydrogen 1s electrons to the transition-metal d band and hence decreases the cohesive energy.[1)] This idea was supported by the calculation of Sieradzki and Ficalora.[2)] Losch[3)] presented a model in which the neighboring metal-metal bonds are weakened by impurities from group IV to group VI. Briant and Messmer[4,5)] treated a Ni cluster with S impurity, and a Fe cluster with P impurity, using a cluster method, the result of which supported Losch's model. The second model is called the 'bond mobility model' and was introduced by Haydock.[6)] In this model, strong bonds with covalent character are generated between the impurity and the host metal atoms. Such local strong bonds have a low mobility; under stress, the sliding of dislocations is suppressed and the ductility is reduced. Goodwin *et al.*[7,8)] examined theoretically the embrittlement of Al boundaries by Ge and As impurities and obtained results in support of this model.

For the impurity-promoted grain boundary embrittlement in Fe and Ni, a lot of first-principles calculations have been performed using the full-potential linearized augmented plane-wave (FLAPW) method based on the density functional theory (DFT). The effects of impurities in a Fe boundary, such as P and B,[9)] C,[10)] Mo and Pd[11)] and H,[12)] have been studied in detail. Some additions on the P impurity-promoted embrittlement of the Fe boundary have also been examined, such as Mn[13)] and Mo.[14)] For a Ni grain boundary, the effects of H, B, P[15)] and Li, He, Ca[16)] have been investigated. The results show that the segregation of typical embrittling elements such as P and H in Fe and Ni grain boundaries decreases the cohesion across the boundary. Therefore they can be classified into the 'decohesion model'.

Computational works on the Al grain boundary embrittlement, however, have been limited to the embrittling elements from group III to V of the periodic table. As mentioned above, Goodwin *et al.*[7,8)] examined theoretically the embrittlement of Al boundaries by Ge (group IV) and As (group V) impurities. This seems to be the first DFT calculation on Al boundary. However, the authors did not deal with a real boundary, but rather Al [111] layers as a model of a boundary. Furthermore, Thomson *et al.* carried out the first-principles pseudopotential calculation of the Ga's (group III) behavior in Al boundaries, where the local relaxation effects, vibrational frequencies and a barrier to grain boundary migration have been examined.[17,18)] Ga is an extreme example of an Al boundary embrittler. The mechanism is classified into the 'decohesion model'.

Recently it has been found experimentally that elements from groups I and II also have an embrittling effect on Al grain boundaries. For example, it has been reported that for an Al–Mg alloy, a very small amount of Na[19)] or Ca[20)] promotes embrittlement. By Auger Electron Spectroscopy (AES) detecting, it is found that the embrittlement should result from the impurity segregation at the Al boundary, though Na's content was too lower (<1 mass ppm) probably to detect on the intergranular fracture surface. Hinode *et al.*[21)] reported that the precipitated Si promotes the nucleation and growth of voids in Al conductor films for LSI use and thus degrades the reliability of performance of LSI. Ogata *et al.*[22)] performed the first-principles calculations on the Al $\Sigma = 5$ tilt boundary with a precipitated Si-atom. They found the strong Al–Si bonds at the interface, which seems to prevent relative sliding motion along the grain boundary. Thus the mechanism seems to be classified into the 'bond mobility model'. It would be interesting to see how Si impurity

behaviors on a more complicated tilt boundary like Al $\Sigma = 9$. S also promotes the embrittlement of Al alloys. It has been reported[23] that if a small amount of S was added in Al–Cu alloy aged at 130°C and 190°C, the ductility of Al–Cu alloy decreases significantly. S was detected by AES in intergranular fractal surfaces, which indicates that the embrittlement is caused by the boundary segregation of S in Al.

In order to clarify the embrittlement mechanism of Al grain boundaries promoted by the above impurities, we have undertaken first-principles calculations on the Al grain boundary with these segregated impurities. It is of great interest to compare the mechanism of the embrittlement by each species with each other. Preliminary accounts have been published.[24–27] In this paper we summarized the effect of these impurities on an Al grain boundary and discuss the differences among those.

2. The Supercell and the Computational Method

We deal with an Al $\Sigma = 9$ $(2\bar{2}1)/[110]$ tilt grain boundary, which is a typical coincidence boundary in Al. It is formed by rotating a grain by 38.94° along the [110] axis, and $(2\bar{2}1)$ is set as the boundary plane. The supercell is constructed as shown in Fig. 1. The coincidence site lattice (CSL) supercell on the boundary plane is defined by $\frac{3\sqrt{2}}{2}a_0[\bar{1}\bar{1}4]$ and $\frac{\sqrt{2}}{2}a_0[110]$. The length in the [110] direction is set to be twice that of the CSL, *i.e.* $\sqrt{2}a_0$, in order to isolate impurity atoms and to retain the symmetry of the configuration. In the $[2\bar{2}1]$ direction, two symmetric boundaries are introduced to make the three-dimensional periodicity.

We used the first-principles plane-wave pseudopotential method[28] based on DFT[29,30] with the local density approximation (LDA).[31] We constructed the pseudopotentials for Al[32] and S[33] using the Troullier-Martins scheme,[34] for Na,[35] Ca (cutoff radii: 1.72, 2.41, 1.95 a.u.) and Si[36] using the Hamann-Schlüter-Chiang scheme.[37,38] For Na and Ca, we used the partial core corrections.[39] We used the separable form by Kleinman and Bylander[40] with the p orbital as the local component. The lattice parameters calculated from the pseudopotentials are 0.395, 0.398, 0.539 and 0.537 nm for fcc Al, bcc Na, fcc Ca and diamond Si, respectively, which are in good agreement with the corresponding experimental values 0.402 (0 K),[41] 0.4225 (5 K),[42] 0.558 (298 K)[42] and 0.5429 nm (0 K).[43] The lattice parameter of ZnS agrees with the experiment.[33] The agreement indicates that the calculated pseudopotential of S is good.

The electronic ground state is obtained efficiently using the conjugate-gradient technique proposed by Bylander, Kleinman and Lee[44] with the Kerker mixing scheme.[45] This method has been shown to be very efficient for determining the minimum of the Kohn-Sham energy functional for large systems containing metallic bonding.[46] The plane-wave energy cutoff is 13 Ry, and 32 k-points in the Brilliouin zone were used. The valence charge density is determined on a real-space FFT grid of $128 \times 64 \times 32$ points. All the atoms were relaxed according to the Hellman-Feynman forces until all these forces were less than 0.5 eV/nm.

We first calculated the relaxed atomic configuration of the clean Al grain boundary. The obtained reconstructed configuration is consistent with high-resolution transmission electron microscopy (HRTEM) observations,[47] as shown in Fig. 2.

We choose 4 equivalent sites of the impurity substitution in the boundary, as shown in Fig. 1. In this configuration, the impurity atoms can be isolated without neighboring to each other and the symmetric property can be kept.

It should be noted that the position changes along the z direction (*i.e.*, fcc Al [110] direction) occur for the atoms on the (110) planes in the configuration with impurity atoms, although the configuration of the clean boundary has no such displacements due to the symmetric property. For the configuration with impurities, the displacements on the planes B and D in Fig. 1 are almost zero because of the symmetric property of the supercell. The displacements on the (110) planes A and C in Fig. 1 are substantial, because the presence of impurities on the planes B and D affects the

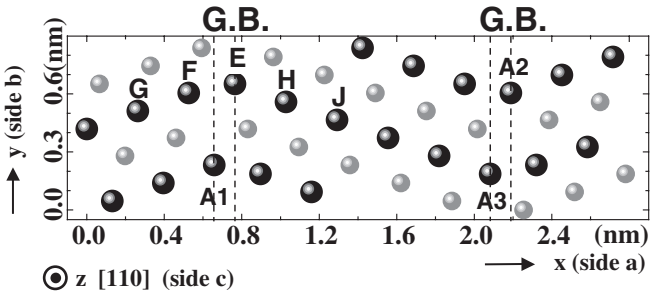

Fig. 1 Cross-section of the [110] direction of the supercell of Al $\Sigma = 9$ $(2\bar{2}1)/[110]$ tilt grain boundary. The lengths of the sides *a*, *b*, *c* are 2.8469, 0.8379 and 0.5586 nm, respectively. There are 84 atoms in the supercell. G, F, E, H, and J are atom positions marked for later reference. There are 4 atomic layer in the supercell, *i.e.* 1st layer A, 2nd layer B, 3rd layer C and 4th layer D. The dark-grey spheres indicate atoms of the B (or D) layer in the supercell, while the light-grey spheres indicate atoms of the A (or C) layer in the supercell. In the impurity segregation case, 4 Al atoms, E and A3 in the B layer, A1 and A2 in the D layer, are replaced by the impurity atoms.

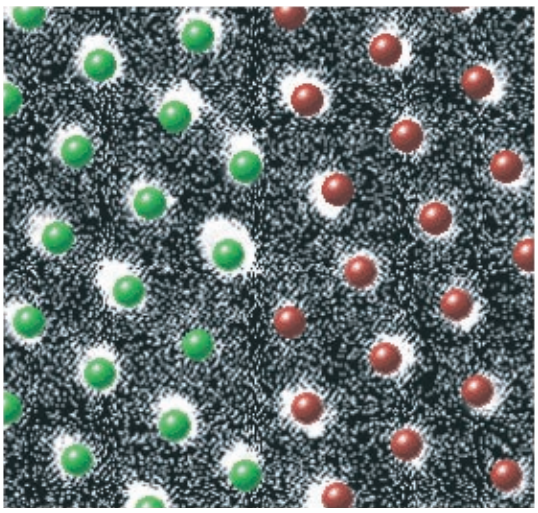

Fig. 2 Direct comparison between the obtained reconstructed configuration (indicated with green and red spheres) and the high-resolution transmission electron microscopy (HRTEM) image for Al $\Sigma = 9$ $(2\bar{2}1)/[110]$ grain boundary.

atomic positions on the adjacent (110) atomic planes, namely A and C. However, even in these two planes, the atomic position change of z coordinate is lower than 0.002 nm in all the four cases, *i.e.* Na, Ca, Si and S segregation cases. In the Si and S cases, the atomic position change is much more lower than that of the Na and Ca cases. Note that the plane space in (110) direction is about 0.142 nm. The FFT mesh in this direction is 32, thus the mesh space is 0.018 nm. We can see that displacement in z direction is smaller than 1.5% of the plane space and 1/9 of the mesh space. Thus relaxed configuration and charge density distribution are mainly analyzed on the x-y plane, *i.e.*, (110) plane.

3. Results and Discussion

3.1 Na and Ca segregation

Figures 3(a) and (b) shows the relaxed atomic configurations for the Na and Ca substitution cases, respectively. We plot only the left half part of A and B layers because the symmetry dictates the other half. E is the position of the impurity atom in the segregation case. The distances between the atoms indicated by G, F, E, H and J are calculated (including small change in the z coordinate) and listed in Table 1. For both the Na and Ca segregation cases, Al atoms around the Na or Ca atom move away from the Na or Ca atom compared with the relaxed configuration of the clean boundary. The displacements in the case of Ca are larger than those for Na. For example, the distances between the impurity atom and the adjacent host atom in the B layer, $EF_{Ca} = 0.2803$ nm (7% increase) $> EF_{Na} = 0.2719$ nm (4% increase) $> EF_{Al} = 0.2622$ nm; $EH_{Ca} = 0.3004$ nm (9% increase) $> EH_{Na} = 0.2919$ nm (6% increase) $> EH_{Al} = 0.2764$ nm. On the other hand, the distances between the adjacent Al atoms and the back Al atoms, namely FG and HJ, both decrease as compared with those of the clean boundary. According to the periodic conditions of the CSL, position changes in the y and z directions will not contribute to the change of boundary volume. Because the size in the x direction in the supercell is fixed, the present change of boundary volume should be different from that of a real case. However, from the distance enlargement between Al and impurity atoms in the boundary, it can still be concluded that, even in a real case, the boundary volume should be enlarged by Na or Ca segregation, and that the boundary expansion by Ca segregation should be greater than that by Na's.

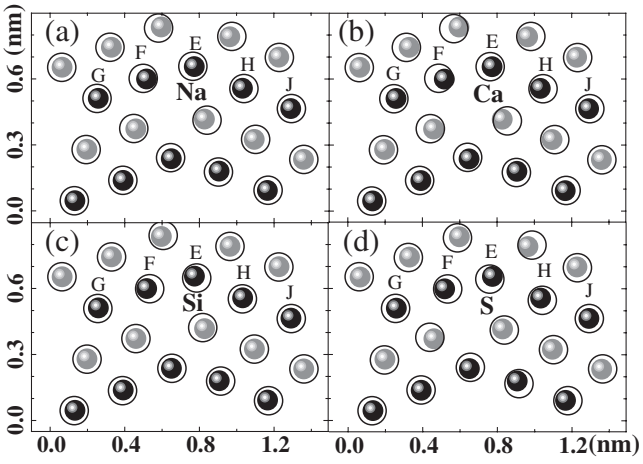

Fig. 3 Relaxed configurations of the left-half part of layer B and A in the supercell. Atom positions without impurity segregation are represented by small spheres, in which the dark-grey and the light-grey ones represent the atom positions of the B and A layers, respectively. Large circles indicate atom positions with impurity segregation. (a) Na segregation (b) Ca segregation (c) Si segregation (d) S segregation. The displacements of Si and S have been enlarged 5 times so it can be seen clearly.

Table 1 Interatomic distances (nm) between Al atoms, or Al and impurity atoms (The letters G, F, E, H and J refer to atomic positions illustrated in Fig. 1).

	Al[a]	Na[b]	Ca[c]	Si[d]	S[e]
FG	0.2736	0.2639	0.2583	0.2772	0.2774
EF	0.2622	0.2719	0.2803	0.2611	0.2558
EH	0.2764	0.2919	0.3004	0.2737	0.2806
HJ	0.2748	0.2704	0.2667	0.2753	0.2729

[a]clean boundary [b]Na segregation [c]Ca segregation [d]Si segregation [e]S segregation

The difference in the interatomic distances around the impurity atoms in the relaxed configurations can be explained by the atomic radii or atomic volumes of Al, Na and Ca in the metallic state. Because the interactions between Al and Na or between Al and Ca are not so significant, Na or Ca atoms in Al boundaries tend to have similar atomic radii to those in pure Na or Ca metals. Atomic radius can be defined as one-half of the nearest-neighbor distance in the ground-state configuration of Al, Na or Ca calculated by the present theoretical scheme. They are 0.140 nm for fcc-Al, 0.178 nm for fcc-Na and 0.191 nm for fcc-Ca, respectively. The atomic radius of Al is smaller than that of both Na and Ca, and that of Na is smaller than that of Ca. This clearly explains the present relaxed configuration results.

Figure 4 shows the valence charge density integrated on the y-z plane, which is parallel to the grain boundary plane

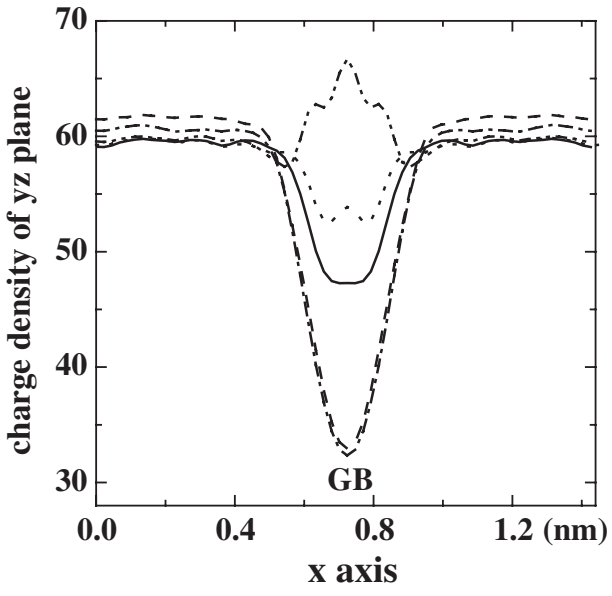

Fig. 4 Integrated charge density on the y-z plane in the left-half part of the supercell. Solid and dotted-dashed, dashed, dotted and dashed-dotted-dotted lines represent clean and Na, Ca, Si, S segregated case, respectively.

$(2\bar{2}1)$, as indicated in Fig. 1. Only the charge density of the left half-part of the supercell was plotted. For both the Na and Ca segregation cases, the charge density in the boundary region is much lower than that in the case of no impurities. In the bulk region, there is a small increase of charge density for the both cases, and the increase for Ca is higher than that for Na.

We plot the contours of the valence charge density distribution of layer B and A in Fig. 5 and Fig. 6. Figure 5 shows the charge density on the layer B containing the impurity atoms, while Fig. 6 shows the charge density on the layer A containing no impurity atoms. Comparing Figs. 5(b) and (c) with Fig. 5(a), it can be said that the charge density decreases significantly in the area near the substituted Na or

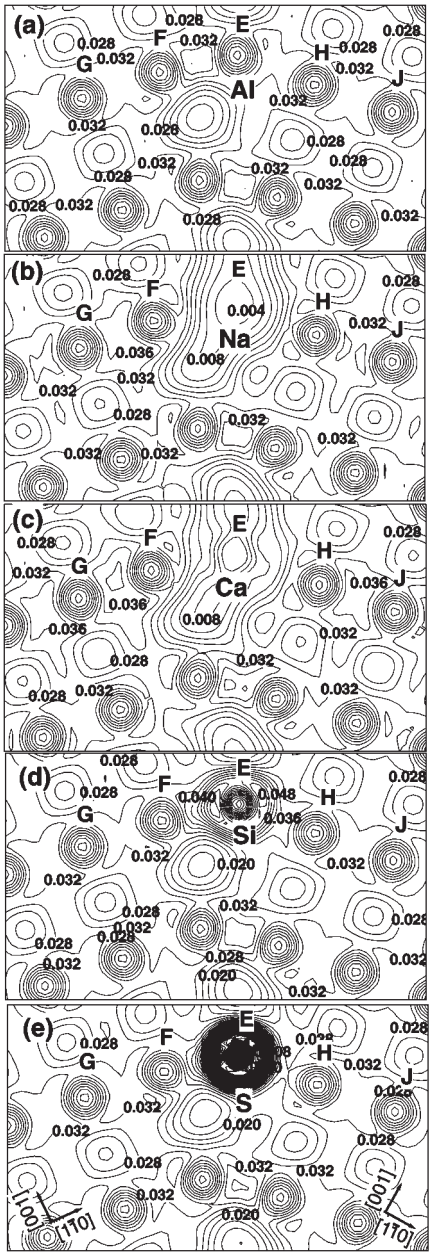

Fig. 5 Contours of the valence charge density of the left-half part of layer B. The interval of the contours is 0.004 e/(a.u.)^3. [1$\bar{1}$0] and [001] indicated in the figure are lattice directions in the grains. (a) Clean boundary (b) Na segregation (c) Ca segregation (d) Si segregation (e) S segregation.

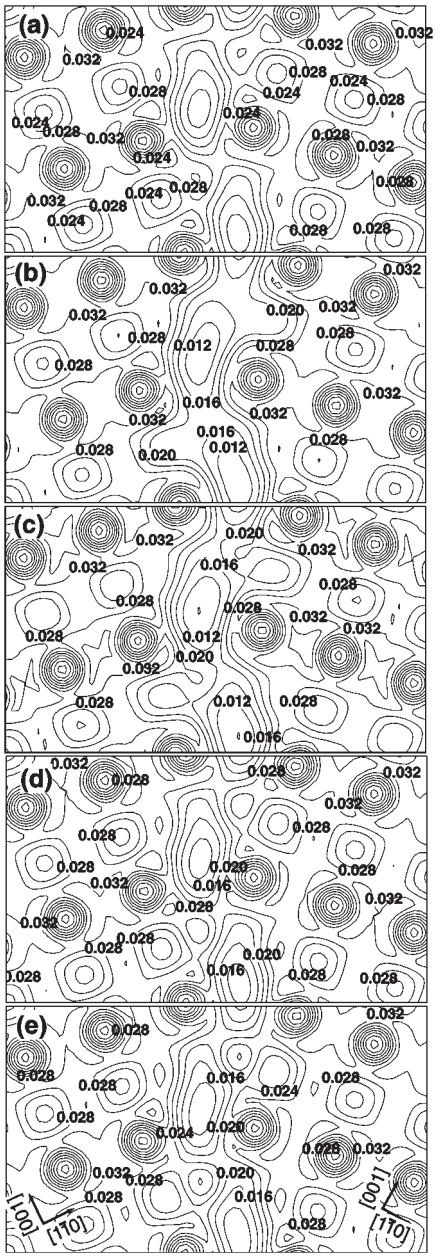

Fig. 6 Contours of the valence charge density of the left-half part of layer A. The illustration is the same as that in Fig. 5.

Ca atom in the layer B (indicated E in the figures). However, in the bulk region there is an increase of charge density between adjacent Al atoms, especially along the [1$\bar{1}$0] directions. As for the charge density in layer A, shown in Figs. 6(b) and (c), we can see that, even though there are no segregated impurity atoms in this layer, the charge density still decreases along the boundary, and the charge density between adjacent Al atoms in the bulk becomes higher especially along the [1$\bar{1}$0] direction. The figures also show that the charge density at the boundary in the case of Ca segregation in the boundary is slightly higher than that of the Na case.

An explanation for the present results of the valence charge density distribution is as follows. First, Al has three valence electrons, while Na has one and Ca has two. These differences should be the main reason causing the charge

density decrease in the boundary region. Ca has one more valence electron than Na; therefore the charge density in the boundary for the case of Ca is slightly higher than that in the case of Na. Second, as mentioned above, because of the different atomic radii of Al, Na and Ca, segregation of Na or Ca atoms causes the boundary to expand and the distances between the neighbor Al atoms and the back Al atoms to decrease, especially along the $[1\bar{1}0]$ direction. The boundary expansion induces a further decrease of the charge density in the boundary region. The decrease in the distances between Al atoms in the bulk region causes the charge density increase in this region, especially along the $[1\bar{1}0]$ direction. Of course, the increase of the charge density in the bulk region for both the Na and Ca segregation should be affected by the fixed cell size in the x direction as mentioned above. If the size in the x direction is enlarged to relax stress, there may be a charge density increase only near the boundary.

Figure 7(a) shows a cross section in the z direction of the supercell, which is perpendicular to the boundary plane $(2\bar{2}1)$. Local density of states (LDOS) is calculated as the sum of two symmetric regions: I and II containing the two interfaces. Figure 7(b) shows the results of LDOS. All of the LDOS of the three cases, *i.e.* clean and Na, Ca segregated case, basically have the features like the DOS of free electrons. This means that the atomic bonding at the boundary is mainly metallic for all the three systems and that there exist no significant ionic or covalent interactions even in the systems with impurities. However, for the Na and Ca segregation cases, the LDOS decreases over the whole energy region compared with that of the clean boundary, although there exists a peak above the Fermi energy for the case of Ca. This peak is caused by the 3d state of Ca.[48)]

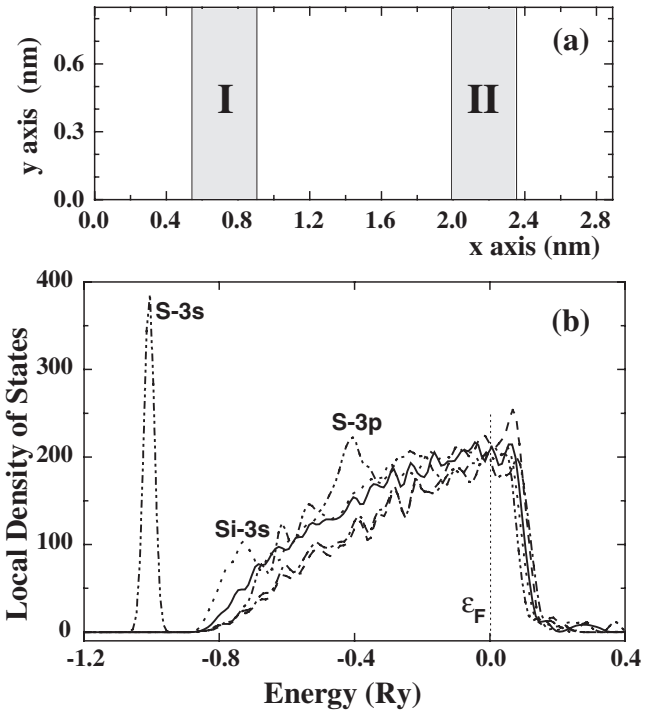

Fig. 7 (a) Illustration of the calculation ranges for the LDOS. (b) LDOS of the range above. Solid and dotted-dashed, dashed, dotted, dashed-dotted-dotted lines stand for clean and Na, Ca, Si and S segregated case, respectively. The Fermi energy is indicated by ε_f.

Therefore, both Na and Ca segregation cause the boundary expansion and the significant decrease of charge density around the impurity atoms and along the boundary. The significant decrease of the valence charge density in the Al boundary means the formation of weak bond regions between grains. As compared with the clean boundary, there exist several weak impurity-Al bonds and Al–Al bonds at the boundary. Such weak-bond regions should act as the origins of the crack or the preferential path of the cracks under stress. This is an impurity-promoted embrittlement mechanism by the Na (group I) and Ca (group II) segregation. It can be said that the mechanism is classified into the 'decohesion model'. However, as discussed above, there are some new features which are quite different from previous examples of the 'decohesion model'. For example, the impurity-Al bonds have basically metallic characters, and the low charge density region is formed between Al atoms and impurity atoms, and also between grains, in contrast to the Losch's model in which the decohesion occurs between neighboring metal-metal atoms by elements of IV, V and VI groups.

3.2 Si Segregation

The relaxed atomic configuration by Si segregation is shown in Fig. 3(c). E is the position of Si atom in the substitution case. The interatomic distances among the five atoms (G, F, E, H and J) are listed in Table 1. As shown in the figure, Al atoms around the Si atom (E) get nearer to the Si atom compared with the relaxed configuration of the clean boundary (as in Table 1: $EF_{Si} = 0.2611\,\text{nm} < EF_{Al} = 0.2622\,\text{nm}$, 0.4% decrease; $EH_{Si} = 0.2737\,\text{nm} < EH_{Al} = 0.2764\,\text{nm}$, 1.0% decrease). The distance between the adjacent Al atoms becomes greater (as in Table 1: $FG_{Si} = 0.2772\,\text{nm} > FG_{Al} = 0.2736\,\text{nm}$, 1.3% increase; $HJ_{Si} = 0.2753\,\text{nm} > HJ_{Al} = 0.2748\,\text{nm}$, 0.2% increase). From the distance decrease between Al and impurity atoms in the boundary, it can be concluded that the volume of the boundary should be reduced by the Si segregation, although the present fixed size of the supercell prevents the quantitative determination of such effects similarly to the Na and Ca cases.

For the integrated valence charge density on the y-z plane in Fig. 4, the charge density at the boundary is higher than that of the clean boundary, and in the bulk region there is no obvious charge density change.

Figure 5(d) shows the charge density on the layer B containing Si atoms, while Fig. 6(d) shows the charge density on layer A containing no Si atoms. The results are quite different from that of the Na and Ca segregation cases. Comparing Fig. 5(d) with Fig. 5(a), it can be said that the charge density is much higher around the Si atom (E), especially between the atoms E and F. There is no obvious charge density change between the Al atoms in the bulk part of this layer. Comparing Fig. 6(d) with Fig. 6(a) it can be seen that there is no obvious change of the charge density in layer A. The charge accumulation is mainly localized between the Si atom and the neighboring Al atoms.

A Si atom has 4 valence electrons, more than that of an Al atom, which causes charge increase around the Si atom. The boundary contraction induces a further charge density increase between the Si atom and adjacent Al atoms.

In Fig. 7, there is an obvious increase of LDOS for the Si segregation case near the bottom of the LDOS. This means that there exists a stronger bond with some covalent characters in the grain boundary. This is consistent with the charge distribution results.

It can be concluded that there exist stronger Si–Al bonds in the boundary than the metallic Al–Al bond. This point is clear by the great increase of the charge density and the contraction of distances between the Si atom and neighboring Al atoms especially E–F bond of obvious directional bond charge. Note that Si is a typical covalent binding element. The covalent bond is more directional, and is generally stronger than the metallic bond. Therefore the stronger Si–Al bonds should have the mixture of covalent and metallic characters. The center of gravity of these bonds deviates to the atom E, *i.e.* the Si atom. Such bonds should have localized, rigid and directional character, thus prevent the rearrangement of atoms under stresses. Note that there is no obvious charge density decrease around the boundary. Therefore, the mechanism of the embrittlement by Si segregation is classified into the 'bond mobility model'.

3.3 S Segregation

The relaxed atomic configuration is shown in Fig. 3(d) for the S segregation case. The interatomic distances among the five atoms (G, F, E, H and J) are listed in Table 1, where $EF_S = 0.2558\,nm < EF_{Al} = 0.2622\,nm$, 2.4% decrease; $EH_S = 0.2806\,nm > EH_{Al} = 0.2764\,nm$, 1.5% increase. The Al atom F neighbor to the S atom E gets nearer to the S atom compared with the relaxed configuration of the clean boundary. On the contrary, it is very interesting that the Al atom H gets farther away from the S atom E. This is different from both the Na or Ca case (the distances of EF and EH both increase) and the Si case (the distances of EF and EH both decrease). The figure also indicates that only the distance of EF becomes shorter. The distances between E and other Al atoms all become larger.

As for the integrated valence charge density on the y-z plane shown in Fig. 4, the charge density of the S segregation case is much higher at the boundary than that of the clean boundary. In the bulk region, there is no obvious change of valence charge density, similar to the Si case.

About the valence charge density distribution on the layer B shown in Fig. 5(e), it can be said that the charge density is much higher between the S atom E and the Al atom F. However, the charge density is lower between S atom E and Al atom H than that of the pure boundary. The charge distribution between the E and F atoms is directional and deviates to the S atom. About the charge density on the layer A shown in Fig. 6(e), there is no significant change. It can be said that the charge accumulation is mainly localized around the S atom E, and between the S atom and the neighboring Al atom F.

S atom has 6 valence electrons, more than that of an Al atom. This causes significant charge increase around the S atom and between the S atom and the adjacent Al atom F. The distance decrease of EF induces a further charge density increase between the E and F atom.

Figure 6(b) shows that there is a peak in the middle energy region (about −0.4Ry) for LDOS of the S case. This peak is caused by the 3p orbital of S. It seems that the 3p electrons of S participate in the stronger S–Al bond. There is another sharp peak of LDOS below the bottom of LDOS of the clean Al boundary. This peak corresponds to the 3s orbital of the S atom, which means the 3s electrons of S do not participate in the S–Al bond.

From all the results for the S segregation case, it can be said that the strong S–Al bond with covalent and metallic characters is formed between S atom and Al (E). However, no strong bonds are found between S and other Al atoms. It is of great interest that S forms a strong bond with only one neighbor, differently from Si. This feature may be caused by the nature of S of group VI. About the mechanism of embrittlement, it is not so easy to determine it from the present results. Both the 'decohesion model' and the 'bond mobility model' seem to be concerned with the S segregation case.

Although the embrittlement mechanisms of Al grain boundaries promoted by the impurities have been examined from the electronic and structural properties in the ground state as discussed above, '*ab initio* tensile test'[49–51] and '*ab initio* shear test'[52–54] based on Nielsen and Martin scheme[55,56] is necessary to be performed so as to make quantitative investigations on the embrittlement mechanisms. The preparing work is underway.

4. Summary

The electronic properties of an Al $\Sigma = 9$ tilt grain boundary with segregated impurity atoms have been calculated by using the first-principles pseudopotential method based on the density functional theory (DFT) and the local density approximation (LDA). The impurities we chose are Na (group I), Ca (group II), Si (group IV) and S (group VI).

Segregation of Na or Ca atoms in Al boundaries induces an increase of boundary volume because of the larger atomic radius, and causes a significant decrease of charge density around the impurity atoms and along the boundary plane, because of the lower valence numbers of the impurity atoms and the expansion of the boundary. The significant decrease of the valence charge density in the boundary means the formation of weak bond regions between grains. As compared with the clean boundary, there exist several weak impurity-Al bonds and Al–Al bonds at the boundary with the segregated impurities. Such weak-bond regions should act as the origins of the crack or the preferential path of the cracks under stress. This is an impurity-promoted embrittlement mechanism by Na (group I) and Ca (group II) segregation. The mechanism is classified into the 'decohesion model'.

Si and S segregation both causes an increase of charge density between Si or S atom and the neighboring Al atom. There forms a bond stronger than metallic bond between the impurity atom and neighboring Al atom. This kind of bond should be a mixture of covalent and metallic characters due to the typical covalent binding nature of Si and S. The bond should have localized, rigid and directional characters, and thus prevent the rearrangement of atoms, such as sliding under stress. However, different from the Si case, S atom forms the strong bond with only one neighbor. Other S–Al bonds seem to be weak because of the charge density

decrease and the distance increase. In this way although the mechanism of embrittlement promoted by the Si segregation can be classified as the 'bond mobility model', it is not so easy to determine that promoted by the S segregation.

In any case, it is of great importance to perform '*ab initio* tensile test' and '*ab initio* shear test' of grain boundary with impurities so as to determine the mechanism of the embrittlement more accurately.

Acknowledgements

The research is supported by the Science and Technology Agency of Japan as joint research with the National Institute for Materials Science (NIMS), and partly by the Science and Technology Promotion of Japan. The research is also supported by National Natural Science Foundation of China (NSFC). Grant No. 50201002.

REFERENCES

1) A. R. Troiano: Trans. ASM **52** (1960) 54–80.
2) K. Sieradzki and P. Ficalora: Scr. Metall. **14** (1980) 641–644.
3) W. Losch: Acta Metall. **27** (1979) 1885–1892.
4) C. L. Briant and R. P. Messmer: Phil. Mag. B **42** (1980) 569–576.
5) R. P. Messmer and C. L. Briant: Acta Metall. **30** (1982) 457–467.
6) R. Haydock: J. Phys. C **14** (1981) 3807–3816.
7) L. Goodwin, R. J. Needs and V. Heine: Phys. Rev. Lett. **60** (1988) 2050–2053.
8) L. Goodwin, R. J. Needs and V. Heine: J. Phys.: Condens. Matter **2** (1990) 351–365.
9) R. Wu, A. J. Freeman and G. B. Olson: Science **265** (1994) 376–380.
10) R. Wu, A. J. Freeman and G. B. Olson: Phys. Rev. B **53** (1996) 7504–7509.
11) W. T. Geng, A. J. Freeman, R. Wu and G. B. Olson: Phys. Rev. B **62** (2000) 6208–6214.
12) L. Zhong, R. Wu, A. J. Freeman and G. B. Olson: Phys. Rev. B **62** (2000) 13938–13941.
13) L. Zhong, R. Wu, A. J. Freeman and G. B. Olson: Phys. Rev. B **55** (1997) 11133–11137.
14) W. T. Geng, A. J. Freeman and G. B. Olson: Solid State Commun. **119** (2001) 585–590.
15) W. T. Geng, A. J. Freeman, R. Wu, C. B. Geller and J. E. Raynolds: Phys. Rev. B **60** (1999) 7149–7155.
16) R. W. Smith, W. T. Geng, C. B. Geller, R. Wu and A. J. Freeman: Scripta Mater. **43** (2000) 957–961.
17) D. I. Thomson, V. Heine, M. W. Finnis and N. Marazi: Philos. Mag. Lett. **76** (1997) 281–287.
18) D. I. Thomson, V. Heine, M. C. Payne, N. Marzari and M. W. Finnis: Acta Mater. **48** (2000) 3623–3632.
19) H. Okada and M. Kanno: Scr. Mater. **37** (1997) 781–786.
20) K. Horikawa, S. Kuramoto and M. Kanno: Scr. Mater. **39** (1998) 860–866.
21) K. Hinode, N. Owada, T. Nishida and K. Mukai: J. Vac. Sci. Technol. B **5** (1987) 518–522.
22) S. Ogata, H. Kitagawa, Y. Maegawa and K. Saitoh: Comput. Mater. Sci. **7** (1997) 271–278.
23) K. Horikawa: Ph.D. thesis, School of Engineering, the University of Tokyo (1999) pp. 100–110.
24) A. Suzuki, G.-H. Lu, A. Ito, M. Kohyama and R. Yamamoto: Mater. Trans. JIM **40** (1999) 1193–1197.
25) G.-H. Lu, A. Suzuki, A. Ito, M. Kohyama and R. Yamamoto: Mod. Simul. Mater. Sci. Eng. **8** (2000) 727–736.
26) G.-H. Lu, A. Suzuki, A. Ito, M. Kohyama and R. Yamamoto: Philos. Mag. Lett. **81** (2001) 757–766.
27) G.-H. Lu, M. Kohyama and R. Yamamoto: Mater. Trans. **42** (2001) 2238–2241.
28) See, for example, W. E. Pickett: Comput. Phys. Rep. **9** (1989) 115–197.
29) P. Hohenberg and W. Kohn: Phys. Rev. **136** (1964) B864–871.
30) W. Kohn and L. J. Sham: Phys. Rev. **140** (1965) A1133–1138.
31) J. P. Perdew and A. Zunger: Phys. Rev. B **23** (1981) 5048–5079.
32) J. Hoekstra and M. Kohyama: Phys. Rev. B **57** (1998) 2334–2341.
33) J. L. Martins, N. Troullier and S.-H. Wei: Phys. Rev. B **43** (1991) 2213–2217.
34) N. Troullier and J. L. Martins: Phys Rev B **43** (1991) 1993–2006.
35) M. M. Dacorogna and M. L. Cohen: Phys. Rev. B **34** (1986) 4996–5002.
36) M. T. Yin and M. L. Cohen: Phys. Rev. B **26** (1982) 5668–5687.
37) D. R. Hamann, M. Schluter and C. Chiang: Phys. Rev. Lett. **43** (1979) 1494–1497.
38) G. B. Bachelet, D. R. Hamann and M. Schluter: Phys. Rev. B **26** (1982) 4199–4228.
39) A. G. Louie, S. Froyen and M. L. Cohen: Phys. Rev. B **26** (1982) 1738–1742.
40) L. Kleinman and D. M. Bylander: Phys. Rev. Lett. **48** (1982) 1425–1428.
41) P. K. Lam and M. L. Cohen: Phys. Rev. B **24** (1981) 4224–4229.
42) C. Kittel: Introduction to Solid Physics, seventh edition, (John Wiley & Sons, INC., 1996) 23.
43) M. T. Yin and M. L. Cohen: Phys. Rev. Lett. **45** (1980) 1004–1007.
44) D. M. Bylander, L. Kleinman and S. Lee: Phys. Rev. B **42** (1990) 1394–1403.
45) G. P. Kerker: Phys. Rev. B **23** (1981) 3082–3084.
46) M. Kohyama: Mod. Simul. Mater. Sci. Eng. **4** (1996) 397–408.
47) M. J. Mills and M. S. Daw: Mat. Res. Soc. Sym. Proc. **183** (1990) 15–26.
48) J. A. Alonso and N. H. March: Electrons in Metals and Alloys, (Academic, 1989) 66.
49) V. B. Deyirmenjian, V. Heine, M. C. Payne, V. Milman, R. M. Lynden-Bell and M. W. Finnis: Phys. Rev. B **52** (1995) 15191–15207.
50) M. Kohyama: Philos. Mag. Lett. **79** (1999) 659–672.
51) M. Kohyama: Phys. Rev. B **65** (2002) 184107.
52) D. Roundy, C. R. Krenn, Marvin L. Cohen and J. W. Morris, Jr.: Phys. Rev. Lett. **82** (1999) 2713–2716.
53) D. Roundy, C. R. Krenn, Marvin L. Cohen and J. W. Morris, Jr.: Philos. Mag. A **81** (2001) 1725–1747.
54) D. Roundy and Marvin L. Cohen: Phys. Rev. B **64** (2001) 212103.
55) O. H. Neilsen and R. M. Martin: Phys. Rev. B **32** (1985) 3780–3791.
56) O. H. Neilsen and R. M. Martin: Phys. Rev. B **35** (1987) 9308.